Battery-free NFC sub-ppm gas sensor for distributed gas monitoring applications at room temperature

F. Salehnia, A. Lazaro, *Senior, IEEE*, R. Villarino, M. Lazaro, N. Canyellas, X. Vilanova, E. Llobet, *Senior, IEEE*, and D. Girbau *Senior, IEEE*

***Abstract*—This work proposes a low-cost battery-less near-field communication (NFC) tag for gas sensing based on a resistive gas sensor. A proof-of-concept tag is designed using commercially available off-the-shelf (COTS) components. The energy required for the tag operation comes from the magnetic field generated by the reader, and all the electronics are powered by connecting them to the energy-harvesting output of the NFC integrated circuit. Read ranges up to 25 mm have been obtained with commercial NFC-enabled smartphones. The reading of resistance variations due to the presence of gas is performed using a low-consumption timer. The oscillation frequency of this timer depends on the resistance of the gas sensor and is measured by a microcontroller integrated into the tag. This method does not require any gain adjustment for operation, allowing the use of sensors with different resistance ranges. Low-cost room temperature sensors have been integrated for NO_2 detection in both ppb and ppm ranges using laser-induced graphene (LIG). A detection limit of up to 36 ppb has been achieved. The smartphone transmits the data to a cloud database, allowing users to analyze and post-process the information.**

***Index Terms*—Near-Field communications, Radio Identification, Gas Sensor; NO_2 sensor,laser-induced graphene (LIG), environment pollution, energy harvesting.**

I. Introduction

In recent years, hand-held devices for gas monitoring are getting more and more popular. Gas sensors can be integrated in Wireless sensor networks (WSN) for monitoring different substances whose concentration levels can be dangerous. The data can be collected in the cloud for analysis and computing. However, traditional WSN have important limitations that make their deployment difficult. The access to power supply to bias the electronics and communications systems is still a bottleneck. Battery-powered devices can reduce the cost and time required to install remote network nodes however, battery life introduces severe limitations on such systems. Currently, there are nodes powered by various energy harvesting techniques [1]. However, these do not guarantee the continuous supply of energy, so it is necessary to include some type of system that allows it to be stored. In addition, these energy harvesting systems generally increase the cost of the device and may impose restrictions on the installation or mobility of such nodes. For example, solar panels are used to power nodes in sensor networks but sometimes must remain fixed due to their size and require maintenance as their efficiency decreases due to the presence of dust on the surface. Therefore, WSN nodes equipped with batteries as auxiliary energy storage system is growing, although the problems associated with their toxicity are also growing [2]. Ultimately, pollutants can contaminate the soil, water and air and pose a threat to human life and health [3], [4]. Therefore, the concept of green electronics using biodegradable or recyclable materials and the reduction of batteries are gaining popularity [5], [6]. The solution is to reduce both the number of devices that have batteries and the number of electronic components, encouraging their recycling [4], [7].

In addition to the problem of contamination caused by batteries, their lifetime determines the design of the system, even if the nodes are powered based on energy harvesting techniques. Power limitation requires energy-optimal designs, especially when carrying out wireless data communications, in order to save power thus increasing battery lifetime [8], [9]. These limitations determine the maximum distance that can exist between autonomous nodes in sensor networks, which sometimes implies increasing their number to cover a desired area [9], [10]. Overall, battery-free sensors offer several advantages that make them an attractive option for many different applications, including environmental monitoring, healthcare, and industrial automation.

Near Field Communication (NFC) is a type of RFID (Radio Frequency Identification) technology that allows two devices to exchange data when they are placed close to each other, typically within few centimeters. NFC works through magnetic coupling between the tag and the reader. NFC technology is built into most modern smartphones, therefore NFC-based sensors can be read using these smartphones. This fact is advantageous compared to other RFID systems such passive UHF RFID technology, where specific readers are required, which increases the cost of the overall system. Therefore, NFC-based sensors can reach a great number of potential users and can be integrated into collaborative wireless sensors networks [11], [12], [13], [14].

In addition, NFC based sensors allow for fast and convenient communication between devices, and they are becoming increasingly popular in many diverse applications. Commercial

Manuscript received August 22, 2023; accepted January xx, 2023. Date of publication January xx, 2023; date of current version August 22, 2023. This work was supported by the Spanish Government grant RTI2018-096019-B-C31, grant PID2021-122399OB-I00, funded by MCIN/AEI/10.13039/501100011033 and by the EU's European Regional Development Fund (ERDF). E.L. is supported by the Catalan Institution for Research and Advanced Studies via the 2018 Edition of the ICREA Academia Award. Work funded in part by AEI, grant no. PDC2022-133967-I00.

The authors are with the Electronics, Electrical and Automatics Engineering Department, Rovira and Virgili University, Tarragona, Spain (e-mail: foad.salehnia@urv.cat, antonioramon.lazaro@urv.cat, ramon.villarino@urv.cat, marc.lazaro@urv.cat, nicolau.canyellas@urv.cat, xavier.vilanova@urv.cat, eduard.llobet@urv.cat, david.girbau@urv.cat). The corresponding author is A. Lazaro (e-mail: antonioramon.lazaro@urv.cat).

NFC IC featuring energy harvesting capabilities allows the design of battery-free sensors if the current consumption requirement allows to power-up the electronics from the RF energy harvested[15]. Several works demonstrate the operation of NFC sensors without battery for a number of applications [16], [17], [18], [19]. In particular battery-free electrochemical NFC sensors have arising a great interest for point-of-care [20], [21], [22], [23] and wearable applications[24], [25].

NO_2 (Nitrogen Dioxide) sensors are crucial devices used to detect and measure the concentration of NO_2 gas in the air. As a toxic gas produced by various sources, including combustion engines, power plants, and industrial processes, NO_2 can have serious adverse health effects, particularly causing respiratory problems, as well as exacerbating asthma [26]. In industrial settings, NO_2 sensors play a vital role in monitoring gas levels to ensure worker safety and regulatory compliance. Moreover, they find applications in residential and commercial environments to monitor indoor air quality, especially in areas where NO_2 exposure risk is higher, such as near busy roads or industrial facilities [27]. Two common methods used in NO_2 sensors are electrochemical and optical techniques. Electrochemical sensors measure the current generated when NO_2 reacts with a sensing electrode, while optical sensors detect NO_2 through light absorption. Usually, at the output of these sensors an electrical signal is obtained that can be read by a monitoring device or data logger. However, these types of sensors are often unsuitable for battery-free applications due to the high current draw required for reading.

On the other side, graphene-based sensors have gained widespread interest due to their remarkable ability to function effectively at room temperature [28], making them well-suited for wearable gas sensor applications [29]. However, conventional graphene synthesis methods, such as chemical vapor deposition, micromechanical exfoliation of graphite, and chemical and electrochemical reduction of graphene oxide [30], present challenges related to high cost, mass production, and integration into flexible electronic devices. To address these limitations, a scalable approach for producing and patterning porous graphene films with three-dimensional networks was reported in 2014. This innovative method utilizes a CO_2 infrared laser to induce graphene formation from commercially available polymer films [31]. The resulting laser-induced graphene (LIG) exhibits exceptional characteristics, including high porosity, excellent electrical conductivity, and mechanical flexibility [32]. LIG sensors have been found to consist of few graphene layers with outstanding electrical conductivity, thermal stability, and electrochemical performance [33]. The versatility of LIG has led to its application in various fields, such as microfluidic systems, electronic devices, catalysis systems, water purification, and biosensors, primarily due to its unique properties like three-dimensional microporous structure, excellent conductivity, and its facile laser fabrication process [32], [34], [35]. One particularly promising application of LIG is gas sensing. Its high sensitivity and selectivity have made it a valuable candidate for gas sensing applications [36], [37], [38], [39], [29]. By harnessing the exceptional electrical and structural properties of LIG, gas sensors can detect gases with high precision and reliability.

The primary objective and main contribution of this study is to explore the feasibility of integrating a laser-induced graphene-based (LIG) flexible chemoresistive NO_2 sensor with a low-cost battery-less NFC tag. This work is intended as a proof of concept to demonstrate the potential of this integration of LIG-based sensors with NFC tags powered by energy harvesting, which embed a low-power microcontroller. Due to the limitations of the energy that can be collected, a low-power consumption reading method for small resistance variations is proposed, which is based on measuring the frequency generated by a low-power timer-based oscillator. It is shown that the exceptional electrical conductivity and three-dimensional microporous structure of LIG make it an attractive candidate for enhancing sensitivity and selectivity in NO_2 detection [31], and it is demonstrated that it is an excellent candidate to be integrated in NFC tags. Additionally, its easy and cost-effective laser manufacturing process allows for potential integration into various sensor platforms, including wearable devices and air quality monitors.

The rest of the sections of this paper are organized as follows. Section II describes the proposed solution based on NFC and describes the gas sensor developed for the prototypes. Experimental results are given in section III. In section IV a comparison of the results obtained with other RFID or wireless gas sensors in the literature is performed. Finally, conclusions are provided in section V.

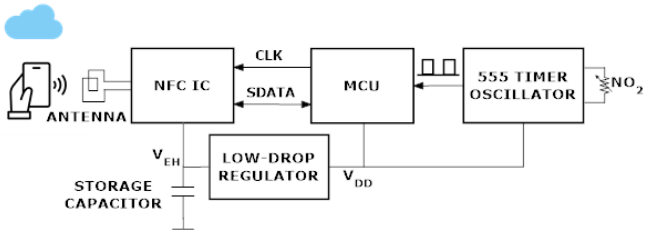

Fig. 1. Block diagram of the proposed system.

II. System Overview

A block diagram of the system is shown in Fig. 1. To measure changes in the resistance of the gas sensor, which depend on its concentration, a signal conditioning circuit is used. There are several methods to measure the resistance but, since the variations are small, Wheatstone's bridge with a differential amplifier would be the common solution [40]. However, due to sensor manufacturing tolerances, the nominal resistance may differ between sensors and the resistive values of the Wheatstone's bridge should be adjusted for each sensor to avoid the saturation of the differential amplifiers. To avoid this drawback, this work proposes another method compatible with low-power designs which also demonstrates good accuracy. It is based on a timer oscillator whose frequency depends on the value of the resistor. The frequency is measured with a microcontroller that stores the data in the EEPROM of the NFC integrated circuit (IC). The data is transferred to the NFC IC via I2C bus and is stored in the standard NDEF text format that can be read from any smartphone equipped with

This article has been accepted for publication in IEEE Journal of Radio Frequency Identification. This is the author's version which has not been fully edited and content may change prior to final publication. Citation information: DOI 10.1109/JRFID.2023.3344636

NFC technology [41], [42]. The system is powered through the energy-harvesting output of the NFC IC (ST25DV04 from ST Microelectronics, which is unregulated and typically provides 3V. To achieve adequate stability, a low-drop regulator that provides 2.7 V at the output is used (TPS76927 from Texas Instruments). It has a maximum current consumption of only 28 μA and a voltage dropout of 71 mV, which guarantees a certain range of security in case of misalignment between the coils of the reader and the tag or in case of detuning effects. A 2 μF bulk capacitor is used as a storage element connected to the energy harvesting output and it is used to reduce the voltage drop during the interrogation by the reader when it is searching for the tags (see [23] for details). The data are sent by the mobile to the cloud database and can be analyzed and post-processed by the users. The most important blocks will be described in more detail below.

A. NO_2 *gas sensor*

The LIG gas sensor is fabricated using a substrate based on a flexible polyimide film (50 µm). Initially, the substrate is cleaned with acetone and then attached to a polyethylene sheet with double-sided adhesive tape. The synthesis of laser-induced graphene is carried out using a CO_2 laser system (SYNRARD 48-2) with a wavelength of 10.6 μm and a maximum power of 25 W. The laser parameters are chosen based on a combination of simulation and empirical results. A MATLAB simulation code has been developed to model the laser writing process for LIG fabrication, taking into account configurable parameters of the laser and fixed specifications such as beam diameter, maximum power, and pulse rise time. This simulation provides various parameters such as laser fluency, power density, and peak power that are critical for understanding the laser-material interaction during the LIG manufacturing process. The MATLAB simulation model is available on GitHub [43]. The laser is focused onto the polyimide surface through a lens with a focal length of 74 mm. The laser beam is scanned over the surface at a speed of 400 mm/s, a frequency of 10 kHz, and a laser power of 20%, with a laser rise time of 40 μs and a beam size of 0.116 mm. The woolly fiber morphology with sheet resistance in the range of $k\Omega/sq$ (2876 Ω/sq) was chosen because it is more suitable for gas sensing applications due to the high porosity of LIG. This precise scanning process allows the selective conversion of the polyimide film into graphene, defining the detection area of the sensor.

Raman spectroscopy analysis is a crucial component of this study to evaluate the quality of Laser-Induced Graphene (LIG) achieved (see Fig. 2). We have focused on the characteristic D, G, and 2D Raman peaks, since they are significant indicators of the graphitic structure and defect density of the LIG samples [44], [45].

In the analysis, the ratio of the intensity of D (defect) and G (graphitic) peaks (ID/IG) is found to be close to 1 for all the LIG samples, suggesting a high level of crystallinity of the LIG, which is essential for the functional integrity of the sensors. This ratio is crucial as it relates to the sp^2–hybridized carbon network and the presence of defects within

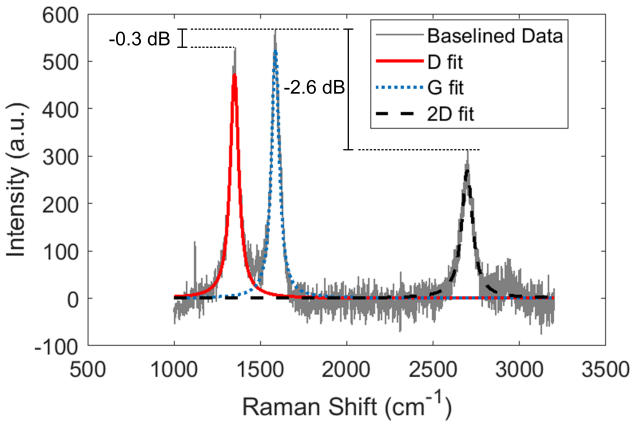

Fig. 2. Raman spectrum of the laser-induced graphene sensor. The baselined data and D, G, and 2D fits are included.

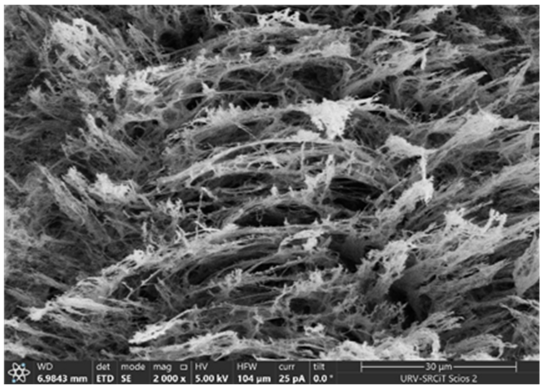

Fig. 3. SEM image of the laser-induced graphene sensor.

the structure. The relatively high ratio indicates that the LIG maintains a balance between the preservation of a graphitic structure and the introduction of beneficial defects that can enhance the material's electrochemical properties. For the LIG samples, it is observed that the D and G peaks appeared at approximately 1345 cm^{-1} and 1580 cm^{-1}, respectively, which are in line with the literature on graphene-like materials. The 2D peak, indicative of the number of graphene layers, is approximately located at 2700 cm^{-1}.

The observation of these well-defined peaks in the Raman spectra of LIG serves as compelling evidence that the material indeed possesses a graphene-like structure, reinforcing its suitability for various applications in the realm of sensor technology and beyond. Meanwhile, SEM (Scanning Electron Microscopy) image in Fig. 3 has further confirmed the formation of a porous structure within LIG, highlighting its unique combination of graphene-like properties and porous architecture, which holds significant promise for gas sensing applications.

A scheme of the LIG sensor is shown in Fig. 4. Their interconnection is designed to match commercial electrode standards to facilitate easy integration with the desired PCB connectors. To achieve this, the electrodes were crafted with dual bases set at an optimal distance of 2 mm apart, aligning with common industrial designs and ensuring compatibility

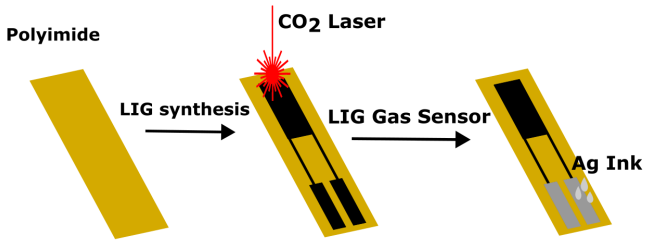

Fig. 4. Laser-induced graphene sensor fabrication scheme.

with standard connectors. Additionally, the manufacturing process involved laser drawing, which imposes certain constraints on the feature sizes that can be achieved. The minimum width that allows forming a uniform layer of LIG is 1 mm. This width is critical for ensuring the structural integrity and uniformity of the conductive paths, which directly influence on sensor performance. To increase the sensitivity of the gas sensor to be able to detect the gas concentration in parts per billion (ppb), a detection area greater than 8 mm^2 is designed. By expanding the sensing area, the sensor can interact with larger number of gas molecules, leading to a better response in front of lower gas concentrations. This increased sensitivity is crucial in applications where detecting trace amounts of gases is of utmost importance. On the other hand, to detect parts per million (ppm) gas concentrations, a detection area smaller than 2 mm^2 is chosen. While the ppb concentration area offers superior sensitivity, the smaller ppm area provides a more suitable range for detecting higher gas concentrations. This dual sensing area design allows the gas sensor to work effectively with different gas concentrations.

Moreover, for ppm concentration, the recovery time of the sensor is significantly reduced. The smaller sensing area allows faster desorption of gas molecules during the recovery phase, leading to faster response times after gas exposure. This attribute is particularly advantageous in applications requiring rapid and repeatable gas sensing performance.

To ensure a reliable connection between the sensing area and the measurement system, a second laser processing step is performed using a speed of 200 mm/s, at a frequency of 12 kHz, and with a laser power of 12%. For this purpose, a more conductive LIG (sheet resistance of 379 Ω/sq) using the least porous cellular network based on the last simulation was chosen. This additional step facilitates the creation of well-defined and conductive pathways, ensuring efficient electrical communication between the sensing area and the measurement system. Furthermore, the addition of silver (Ag) ink in the electrode region of the sensor improves its performance and stability. The Ag ink improves the conductivity as well as the contact of the electrode with the detection area, ensuring accurate and consistent gas detection results. After drop-casting the Ag ink, the sensor is allowed to dry at room temperature for 12 hours, enabling the formation of a stable and conductive layer.

The gas-sensing performance is evaluated in an airtight Teflon chamber with a volume of 35 cm^3 at room temperature (25°C). The sensing chamber is connected to a gas supply and mixing system that uses calibrated gas cylinders and pure dry air (Air Premier purity: 99.999%) as carriers. The resistance of the sensors is then monitored using the battery-less NFC system, in addition to use a multimeter (HP 34972A, Agilent), which records frequency/resistance changes while different concentrations of gases are applied. To reduce the power consumption of the system and to work under more realistic experimental conditions, the total flow is adjusted at a low rate (100 mL/min) using a set of mass-flow controllers (Bronkhorst High-Tech B.V.) and electro valves. The sensors are stabilized under dry air for 30 min before being exposed to a given concentration of a gaseous species for 10 min. The responses to several concentrations are recorded by applying successive dilutions.

B. Sensor readout circuit

The 555 timer is a versatile integrated circuit that can be used to measure resistance and capacitance [46], [47], [48], [49]. A low-power CMOS 555 timer (ICM7555, NXP) is chosen to implement the variable oscillator. A simple square-wave oscillator can be designed with few additional components, whose oscillation frequency is nearly independent of the power supply voltage (unlike the opamp circuit-based oscillator). The current consumption is typically 80 μA at 2.7 V. Other low-power oscillators based on low-power NAND gates can be used as an alternative [50].

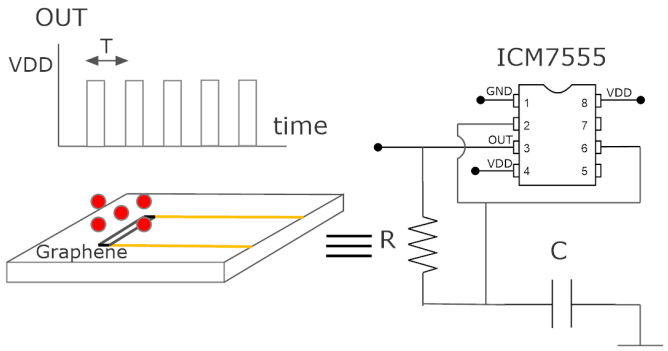

Fig. 5. Schematic of the 555 oscillator used to measure the gas sensor.

The 555 timer is configured as a free-running astable oscillator circuit that connects pin 3 (output) directly to the timing capacitor via a resistor (gas sensor), as shown in Fig.5. When the output at pin 3 is HIGH, the capacitor charges through the resistor. When the voltage across the capacitor reaches $2/3V_{DD}$, pin 6 (Threshold) causes the output on pin 3 to change its state and go LOW. The capacitor now discharges back through the same resistor until pin 2 (Trigger) reaches $1/3V_{DD}$ causing the output to change its state once again. As the capacitor charges and discharges through the same resistor, the duty cycle of the output square wave is very close to 50%. The square wave output pulses have a period equal to approximately $2ln(2)R{\cdot}C$. Therefore the oscillation frequency is given by [51]:

$$f_{osc} = \frac{0.722}{R \cdot C} \quad (1)$$

The output frequency, therefore, depends on the resistance of the gas sensor, which in turn depends on the gas concentration. From the measured frequency, the resistance value can be extracted using (1). The output of the oscillator is connected to a digital input of the microcontroller (MCU), which implements a frequency counter. The gas sensor response is slow, therefore the oscillation frequency can be considered constant during the measurement. A capacitor of C=33 nF is chosen, which results in an oscillation frequency in the order of kHz. The frequency is measured by counting the pulses (N_p) within a time window ($TimeWindow$) and is obtained as:

$$f_{osc} = \frac{N_p}{TimeWindow} \tag{2}$$

By deriving (1), the percent error in the determination of the resistance (ΔR) is the same as that of the oscillation frequency except for the sign:

$$\frac{\Delta R}{R} = -\frac{\Delta f_{osc}}{f_{osc}} \tag{3}$$

A 5 second time window provides a frequency resolution (Δf_{osc}) of 1/5 Hz. For typical oscillation frequencies (see result section) of the order of 15 kHz, the uncertainty in the measurement of the sensor resistance is $\Delta R/R = -1.3 \cdot 10^{-5}$, which is enough for the application.

This method for measuring the frequency is compatible with microcontrollers running at low clock frequencies to reduce power consumption [52]. In the proof of concept, a low-power AVR 8-bit ATTiny1614 microcontroller is used. It has been proven that MCU clock frequency can be reduced down to 1 MHz, it can run from a 1.8 V power supply and draws less than 1 mA at 3 V when set to the lowest clock frequency (i.e. 1 MHz). The microcontroller is programmed using the Unified Program and Debug Interface (UPDI) which is a Microchip proprietary connection for programming and debugging this series of chips. However, other MCUs could be used if they meet the low-power requirements. A delay after power-up is enough for the oscillator to stabilize. After this delay, the counter is enabled. When expires the time window, the MCU stores in the NFC IC EEPROM in NDEF format the measured frequency. The baseline frequency and sensor sensitivity are also stored in the NDEF format, along with a sensor identification number. These configuration data are stored during the sensor initialization procedure by the smartphone. The MCU is programmed in C/C++ language using Arduino IDE environment. The flowchart diagram of the MCU program is shown in Fig. 6.

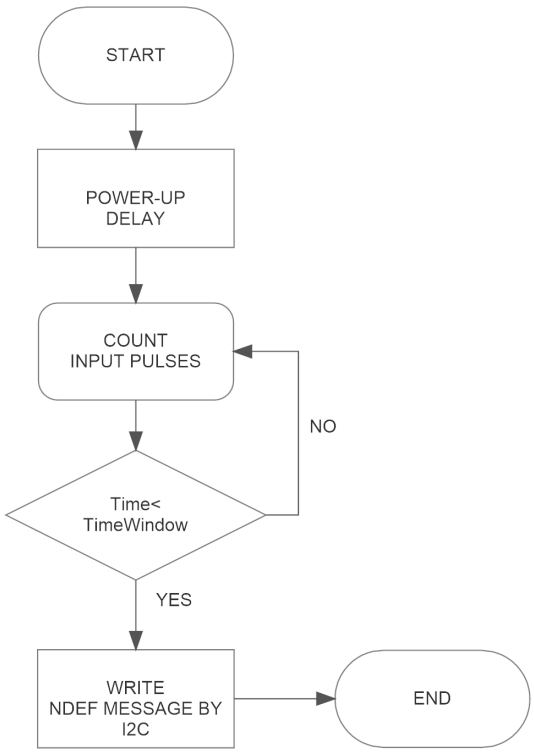

Fig. 6. Flowchart of the microcontroller program.

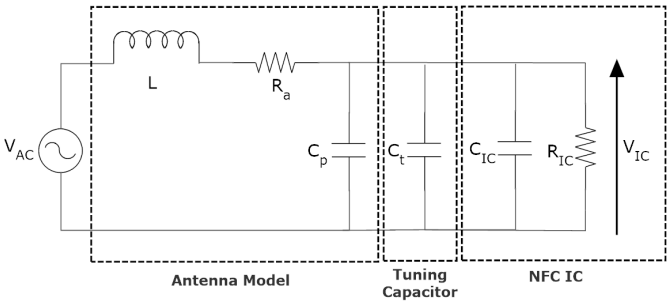

Fig. 7. Equivalent circuit.

C. NFC tag design

Figure 7 depicts the equivalent circuit of the tag including the antenna model, which is composed of the equivalent inductance (L), the antenna resistance (R_a), and the parasitic capacitance due to the microstrip traces (C_p). The NFC IC is modeled around the 13.56 MHz with a capacitance (C_{IC}) in parallel with a resistance (R_{IC}). The RF field generated by the reader induces a voltage in the antenna given by Faradays's law:

$$V_{AC} = j\omega \cdot \mu_0 H \cdot A \cdot N \tag{4}$$

where A is the area of the loop, N is the number of turns, H is the average magnetic field in the tag and μ_0 is the magnetic permeability ($4 \cdot 10^{-7}$ H/m in the vacuum). The maximum efficiency between the reader and the tag is achieved when the tag is resonant. The unloaded resonant frequency of the loop antenna is typically larger than the operation frequency (f_{op}), whose value is 13.56 MHz and is related to the inductance voltage and parasitic capacitance. Therefore, the resonance frequency of the tag can be adjusted to 13.56 MHz by adding an external capacitor called tuning capacitor (C_t). The resonance frequency of the tag is given by:

$$f_r = \frac{1}{2\pi\sqrt{L\left(C_{IC} + C_p + C_t\right)}} \tag{5}$$

Note that the input impedance of the IC is nonlinear and depends on the input power of the tag. However, although the resistance R_{IC} decreases with increasing input power because of the protection limiter on the input of the IC, the capacitance C_{IC} remains approximately constant. The value of this latter is

either provided by the IC manufacturers or can be measured with a VNA or impedance meter. In the case of the NFC IC used in this work (ST25DV04), the manufacturer provides a value of 27.5 pF. In the case of NFC tags with energy harvesting the read range is limited by the voltage required at the input of the NFC IC (V_{min}) to deliver sufficient current to the output of the energy harvesting used to power the rest of the electronics of the tag (MCU and oscillator). Analyzing the equivalent circuit of Fig. 7, it is concluded that the minimum magnetic field amplitude (H_{min}) required is given by [53]:

$$H_{min} = V_{min} \frac{\sqrt{\left[1 - (\frac{f}{f_r})^2\right]^2 + \frac{1}{Q_T^2}}}{2\pi f \mu_0 A N} \tag{6}$$

where Q_T is the total tag quality factor given by:

$$Q_T = \frac{Q Q_L}{Q + Q_L} \tag{7}$$

where Q_L is the quality factor associated to the NFC IC load:

$$Q_L = \frac{R_{IC}}{2\pi f \cdot L} \tag{8}$$

and Q is the unloaded quality factor of the antenna:

$$Q = \frac{2\pi f L}{R_a} \tag{9}$$

From the previous analysis, it can be considered that the tag acts as a filter. If the resonance frequency is tuned to the operation frequency, the minimum field required to power-up the system is minimized. However, a high Q_T value benefits the power transfer and reduces the bandwidth (BW), as can be deduced from (10):

$$BW = \frac{f}{Q_T} \approx 2 \cdot f_{sideband} \tag{10}$$

The tag does not filter the modulated sidebands, therefore the tag quality factor is limited by a maximum tag quality factor. In the case of the tag under standard ISO 15963 (the frequency of the sideband $f_{sideband}$= 13.56 MHz/28), the maximum tag quality factor is 14. Usually, antennas printed on PCB achieve quality factors higher than 14. Therefore, the total quality factor is limited by the load quality factor Q_L. Assuming a value in the order of $R_I C$=525 Ω [54] when the tag is operating in energy harvesting mode, a minimum inductance of 440 nH is required. For inductances greater than this value, the maximum total quality factor requirement can be fulfilled. Note that when the tag is far from the reader (smartphone), the magnetic field is lower than the minimum and the NFC IC does not activate the energy harvesting output. However, if it is within the read range, the tag can respond the queries of the reader and return the previously stored messages in the NFC IC EEPROM. In this situation, the nonlinear resistance R_{IC} is greater than the value reached when the energy harvesting is activated. Therefore, a higher inductance value of about 2-3 times than the minimum value of 440 nH is desirable to not limit the read range. The space limitation in this proof-of-concept prototype is not particularly strict, therefore there is a great degree of freedom in the coil design. In the prototype, a square spiral printed coil with an external length of 40 mm and a total of 6 turns has been designed. Both the width of the traces and the space between them is 0.7 mm. A standard 0.8 mm thick FR4 PCB has been selected, but other substrates, such as flexible substrates, could be considered if required for a particular application. An estimation of the inductance value must be made to obtain an initial value of the tuning capacitor to adjust the tag resonance to 13.56 MHz. The inductance can be estimated using Wheeler's formula [55]):

$$L = K_1 \mu_0 N^2 \frac{D_{av}}{1 + K_2 \rho} \tag{11}$$

The average diameter between the outer diameter and inner diameter D_{av} is given by:

$$D_{av} = (D_{out} + D_{in})/2 \tag{12}$$

The fill factor ρ measures hollowness of the inductor and is defined as:

$$\rho = \frac{D_{out} - Din}{D_{out} + D_{in}} \tag{13}$$

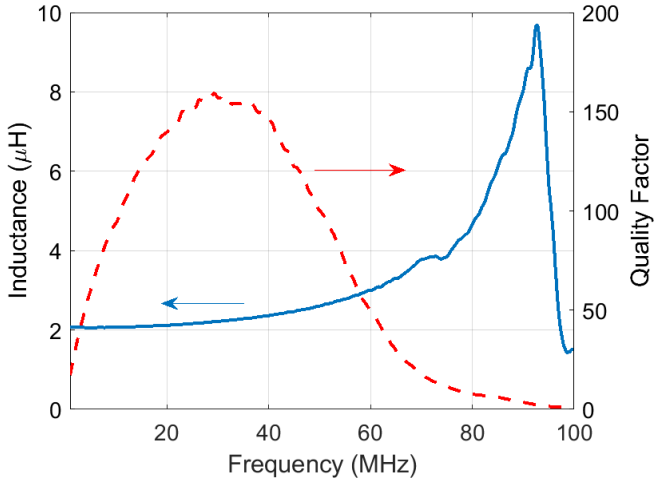

Fig. 8. Measured inductance (left) and quality factor (right)

.

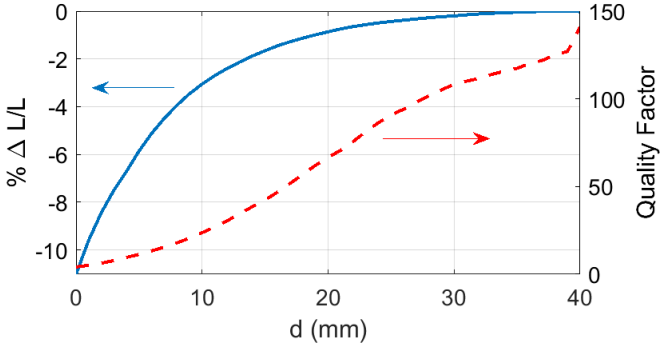

Fig. 9. Variation of the inductance (left) and quality factor (right) with the distance between the tag and the smartphone.

In (11), the coefficients K_1 and K_2 for a square-shaped inductor are 2.34 and 2.75, respectively [55]. The quality factor of the inductance can be obtained from the resistance

TABLE I
MEASURED ANTENNA PARAMETERS.

Distance (mm)	L (nH)	Q	f_r (MHz)	C_p (pF)
10	2.0	75	100	2

of the wire considering the skin effect [56]. An estimated inductance of 2.06 μH is obtained and a quality factor of 134 at 13.56 MHz, which is very close to the value obtained with the full-wave simulator Keysight Advanced Design System (ADS) using the Momentum method (an inductance of 2.09 μH and a quality factor of 136). The measured values are an inductance of 2.082 μH and a quality factor of 129 at 13.56 MHz. From the estimated inductance, the tuning capacitance required to adjust the tag resonance frequency is obtained from 5. However, the presence of metal parts of the smartphone such as the case, battery, and PCB detunes the tag due to the decreased inductance on the tag's own antenna (L). Typically, in modern smartphones, the NFC antenna is composed by a ferrite antenna located over the battery or close to the camera hole. It is necessary to perform an experimental tuning that can be done with the help of a VNA. A test loop antenna is connected to the VNA port to measure the reflection coefficient (S11). This test antenna should be located a few millimeters away to avoid loading the tag. The tag is placed close to the smartphone at the typical read distance (eg. over the tag case). The frequency at the minimum in the measurement of S11 allows to obtain the resonance frequency of the tag, and in this way readjust the tuning capacitance. Fig.8 shows the inductance and the quality factor of a prototype of antenna manufactured using 0.8 mm thick FR4. The inductance has been obtained from the imaginary part of the parameter Z_{11} after de-embedding the delay introduced by the SMA connector used in the characterization with the VNA. The parasitic capacitance (C_p) can be obtained from the measured antenna resonance frequency (f_r) and the extracted inductance.

D. Application (app)

Below the resonance frequency, the coil quality factor increases approximately linearly and is determined from the inductance reactance and the equivalent antenna resistance. This resistance depends on the frequency due to the skin effect and increases with frequency [21]. The presence of the parasitic capacitance between the traces decreases the coil reactance as the frequency increases. This effect produces a peak in the quality factor. To investigate the effect of the proximity of the metal parts of the smartphone, this figure shows the inductance and the quality factor as a function of the distance from a metal plate located below the antenna. The inductance decreases due to the image currents induced in the metal, the losses increase and the parasitic capacitance increases due to the proximity of metal, reducing the resonance frequency of the antenna. Table I summarizes the inductance, quality factor, unloaded resonance frequency, and parasitic capacitance of the antenna in free space (far from metallic parts).

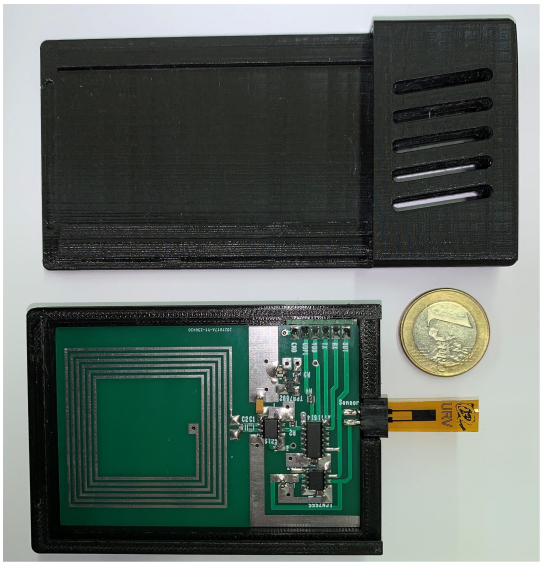

Fig. 10. Prototype with a 3D-printed protection case.

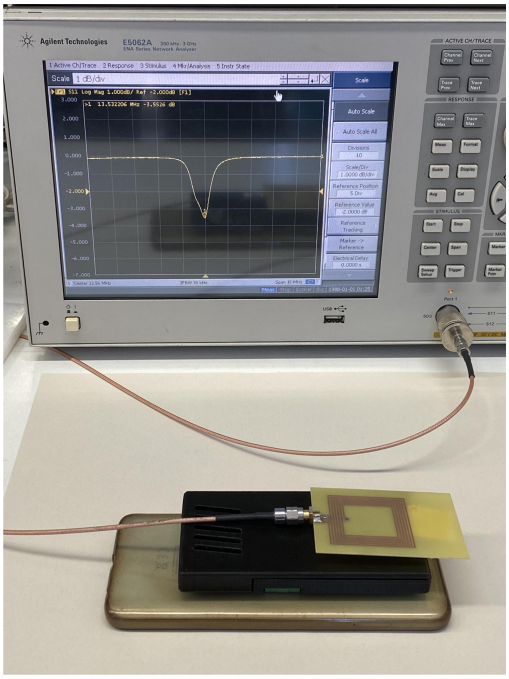

Fig. 11. Setup used to adjust the resonance frequency of the tag using a test antenna connected to the VNA.

Due to the detuning caused by the metal parts of the reader (smartphone), the resonance of the tag must be adjusted to 13.56 MHz using the tuning capacitor and with the help of the VNA in an environment close to the final application (see Fig. 11, which shows the setup used, composed with the test antenna placed close to the tag and the smartphone to power it up). The value of the tuning capacitor found for the designed tag prototype placed on the smartphone was 39 pF (see Fig. 10).

Fig.12 shows the measured average magnetic field for the smartphone used in the experimental tests (Xiaomi Redmi 10) with the setup described in [54]. A multimeter is used to measure the output voltage of the regulator as a function of the

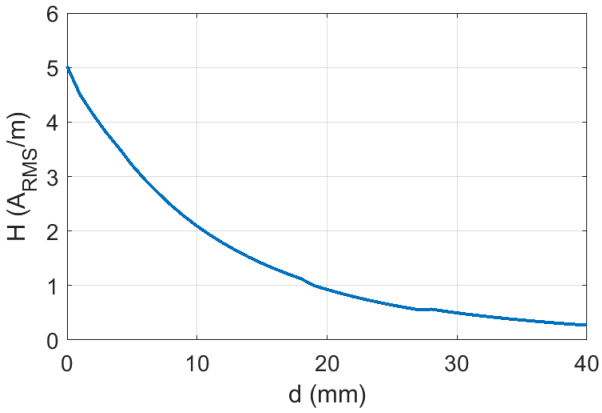

Fig. 12. Measured magnetic field.

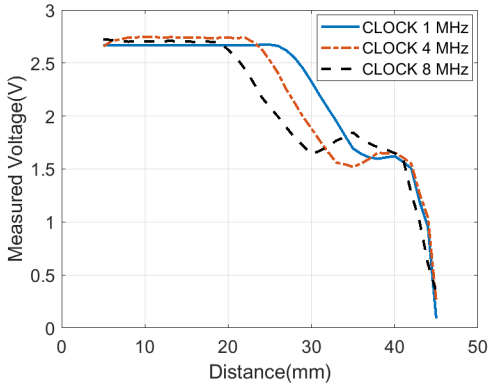

Fig. 13. Measured voltage at the output of the regulator as a function of the distance between the tag and the reader for the clock frequencies of 1 MHz, 4 MHz, and 8 MHz.

distance between the NFC reader (smartphone) and the tag, in order to test the energy harvesting performance. The measured voltages for several MCU clock frequencies are shown in Fig. 13. It is concluded that the tag can operate close to 20 mm at 8 MHz and almost 30 mm at 1 MHz. The difference is attributed to the increase current consumption of the tag caused by the MCU clock frequency. Therefore, it is imperative that the reader provide a minimum magnetic field of 1 A_{RMS}/m.

An application that works under Android operating system has been designed for testing the system. An screenshot of the main window is shown in Fig.14. The app has the option to store the calibration data (polynomial fitting coefficients) in the EEPROM of the NFC IC. The smartphone reads the NDEF text message and makes the necessary calculations to determine the gas concentration. Different databases can be used to upload the data using API REST protocol through the mobile internet connection. The user can select between uploading the data in a ThingSpeak channel from Mathworks, a mySQL database or influxDB. The keys to write to and read from these databases can be set using a configuration menu. Previously stored data can be visualized on the mobile (see Fig. 14) or in a web-based dashboard. In the case of choosing influxDB, Grafana tools are used for visualization in a customized dashboard. Latitude and longitude obtained from the GPS sensor of the smartphone and are stored in the database for future applications where the tag can be placed in different locations or can be mobile.

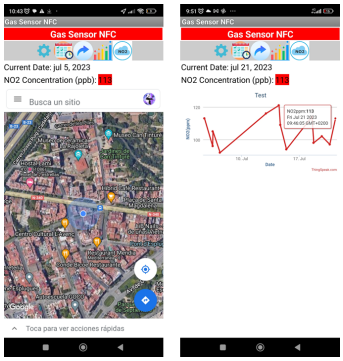

Fig. 14. Screenshot of the Android app designed for testing.

III. Results

The technique can be applied to monitor the air quality in cities, which implies that the system is capable of detecting concentrations of NO_2 lower than 1 ppm. For this purpose, a gas sensor with a sensing area of 8 mm^2 has been designed. After cleaning the sensor with synthetic air for 3 hours, different concentrations of NO_2 have been alternately applied for 600 seconds followed by synthetic air for 1800 seconds. The measured oscillation frequency and the derived resistance from (1) are shown in Fig. 15. The sensor has a nominal resistance of about 1555 Ω obtained from the sheet resistance calculated with the model combining the different LIG traces. Good agreement was obtained with the value of 1590 Ω obtained from (1). From the last figure, the response curve is obtained. The normalized variation of the resistance after exposure to different concentrations is shown in Fig. 16. The result shows the average of 4 exposure cycles. A first-order polynomial has been used to fit the curve. For each concentration, the standard deviation (error bars) between measurements at each exposure cycle performed with the prototype powered by the energy harvesting from the electromagnetic field provided by the smartphone is shown.

The limit of detection (LOD) is obtained using the following expression [57]:

$$LOD = \frac{3 \cdot \sigma}{S} \tag{14}$$

where σ denotes the standard deviation of the response baseline, and S represents the sensitivity (slope) derived from the calibration curve. A LOD of 36 ppb is obtained using (14) from the standard deviation of 0.0254% computed from the variations of the baseline (see inset figure in Fig. 16) and sensitivity of 6.21%/300ppb (slope of Fig. 16).

The response of the sensor to gas concentrations between 5 ppm and 100 ppm is also investigated. In this case, another LIG sensor with an area 2 mm^2 was used. Different gas concentrations are applied for 600 seconds and afterward are cleaned with synthetic air for 1800 seconds. The measured oscillation frequency as a function of time is shown in Fig. 17. From the measured oscillation frequency, the resistance

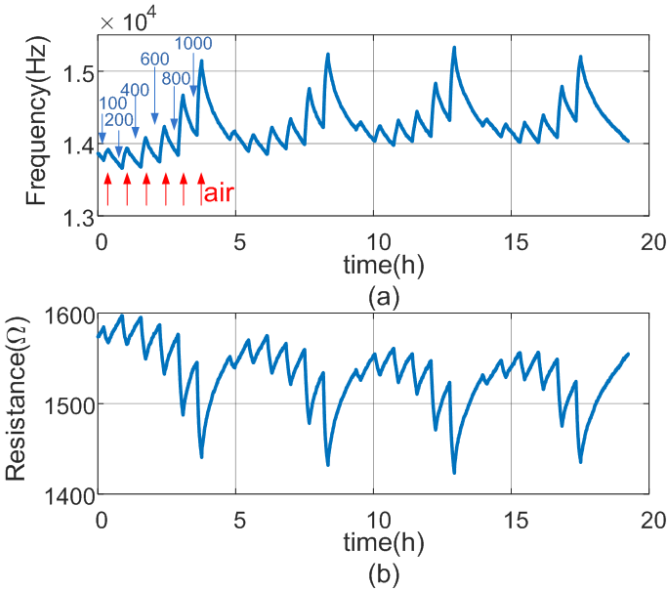

Fig. 15. Response for different NO_2 concentrations of a gas sensor designed for sub-ppm detection. Timer frequency (top) and resistance (bottom) variation as a function of time. The red arrow indicates the injection of air. The exposure and recovery times are 600 and 1800 seconds, respectively. Four exposure cycles are shown and concentration values are given in ppb.

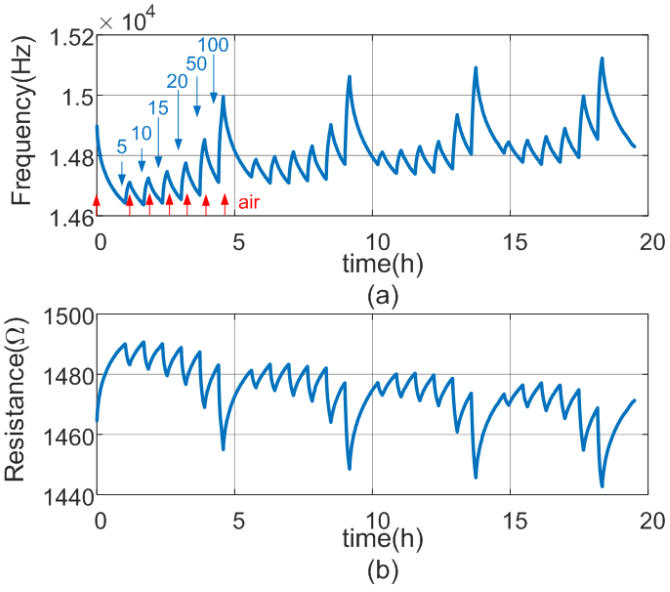

Fig. 17. Response for different NO_2 concentrations for the sensor designed for high gas concentrations. Variation of the timer frequency (top) and resistance (bottom) as a function of time. The red arrow indicates air injection The exposure and recovery times are 600 and 1800 seconds, respectively. Four exposure cycles are shown and concentration values are given in ppm.

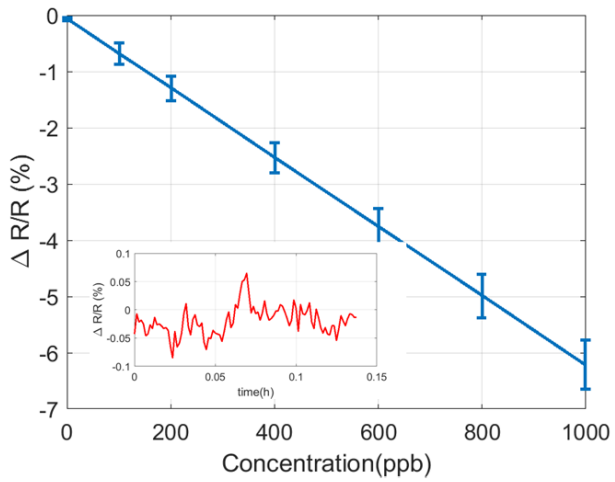

Fig. 16. Normalized variation of the resistance designed for the sub-ppm gas sensor as a function of NO_2 concentration obtained by averaging 4 exposition cycles. The error bar shows the standard deviation between cycles, measured with the prototype with energy harvesting. The inset shows a temporal trace of experimentally recorded noise of the normalized resistance without NO_2.

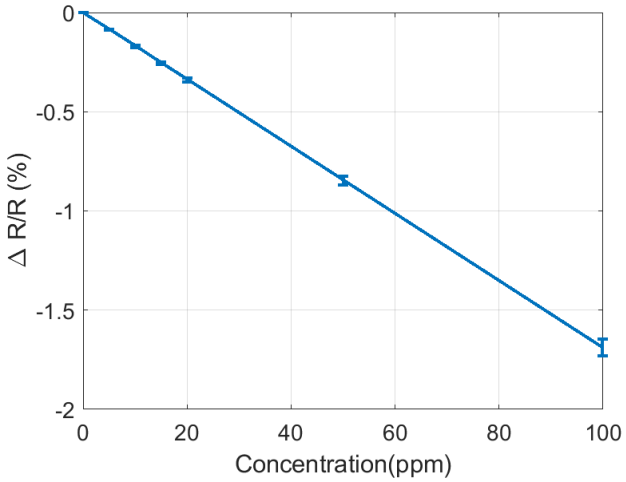

Fig. 18. Normalized resistance variation for the sensor designed for high gas concentrations as a function of NO_2 concentration, obtained by averaging 4 exposure cycles. The error bar shows the standard deviation between cycles measured with the prototype with energy harvesting.

of the sensor can be obtained from (1). A measured value of 1490 Ω was obtained, which agrees with the estimated value of 1587 Ω from the model. The response curve of the sensor for different NO_2 concentrations is shown in Fig. 18. The curve presents a nearly linear behavior in this range. A limit of detection (LOD) of 0.5 ppm is calculated using (14) for this sensor and it can operate up to 100 ppm.

The selectivity test was conducted to assess the sensor's sensitivity to various gases, including CO, NH_3, H_2, H_2S and NO_2. This test, as depicted in Fig.19, involved measuring the percentage change in resistance. The data presented in the figure represents the average of 5 cycles of gas exposure for 30 minutes, followed by sensor cleaning with synthetic air. In particular, the results confirm the high selectivity of the sensor to the NO_2.

The correlation plot showcases the relationship between the normalized resistance of two sensors. These sensors are assessed using both the Agilent system (HP 34972A, Agilent multimeter) and the proposed system with energy harvesting, and they were placed within the same chamber exposed to a NO_2 concentration of 50 ppm for 0.5 hours. The first sensor is connected to the NFC tag, and measurements are taken using a smartphone, which powers the tag by energy harvesting, reads

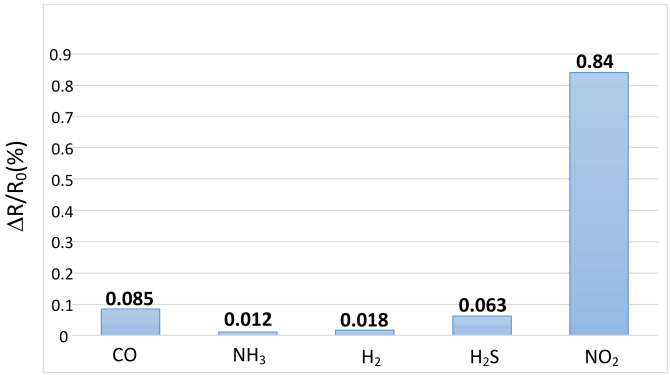

Fig. 19. Gas selectivity when the sensor is exposed to different gases with concentrations of 50 ppm.

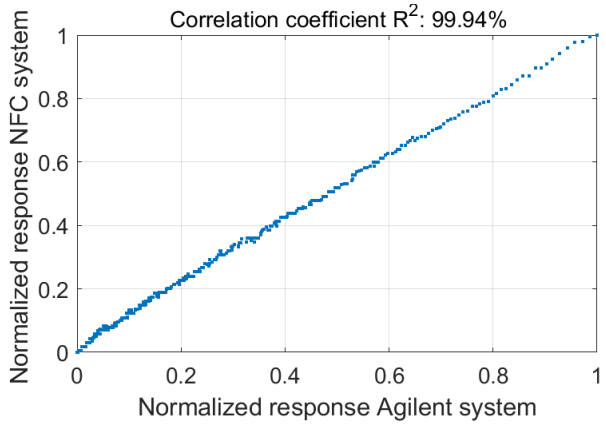

Fig. 20. Correlation plot between normalized response of two sensors exposed to a gas concentration of 50 ppm measured with the Agilent system and NFC-based system.

the measurement from the NFC IC memory, and transmits the data to the database at 10-second intervals. The other sensor is connected to the Agilent multimeter, and the data is sent to a personal computer, allowing synchronized measurement with the first sensor. A high correlation of 99.94% is obtained between the responses of these two sensors (Fig. 20).

Additionally, dynamic responses have been investigated. Figures 21 and 22 show the typical response curve for designed sub-ppm and high concentration ranges. These responses are recorded by subjecting the sensors to step changes of 1 ppm and 100 ppm, respectively, at room temperature (25 °C). The measured response times are 483 seconds and 414 seconds, respectively, and the recovery times are 2689 seconds and 2661 seconds, respectively.

In order to investigate the reproducibility, three sensors have been manufactured and their responses are compared. The sensors are simultaneously exposed to different concentrations in the range between 5 and 100 ppm. Before subjecting the sensors to a new concentration, they are maintained with synthetic air for a recovery interval of 30 minutes. Fig. 23.a shows the frequency variation as a function of time showing a good correlation between the three sensors. The estimated concentration obtained from the calibration curve is shown in Fig. 23.b. Good agreement is obtained, especially for the

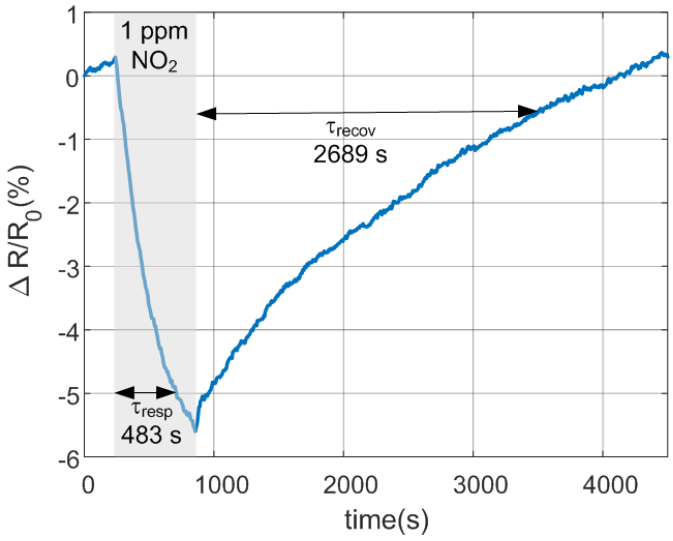

Fig. 21. Typical response curve of the gas sensor designed for sub-ppm detection down to 1 ppm NO_2.

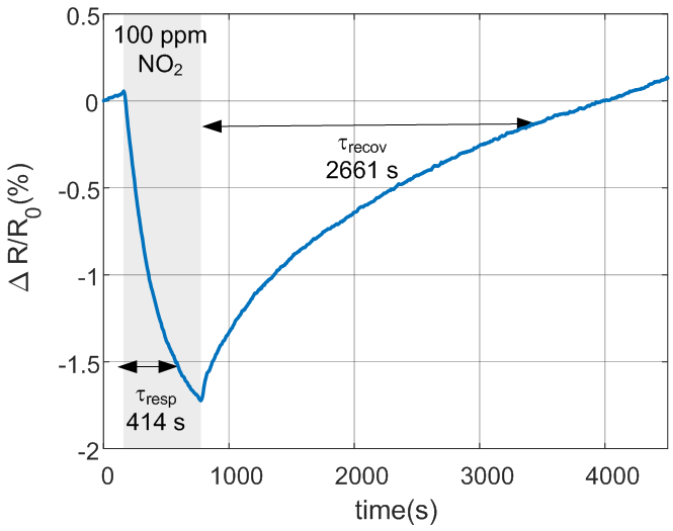

Fig. 22. Typical response curve of the gas sensor designed for high concentration detection up to 100 ppm NO_2.

lowest gas concentrations, where the sensors have enough time to recover the baseline after 30 minutes.

IV. Discussion

This section discusses and compares results obtained with other RFID or wireless gas sensors in the literature. Table II shows a comparison of different parameters such as the presence or absence of battery, communication technology, the detected gas and concentration ranges that can be detected, the sensor technology used, and response times.

There are several examples of sensors developed for the detection of gases using passive UHF RFID. Some of those, based on passive UHF, have been presented in [58], [59], [60], [61], [62]. A gas-sensitive material such as single-channel carbon nanotubes (SWCNT) loads the tag antenna producing a detuning of its the response in the presence of gas. The result

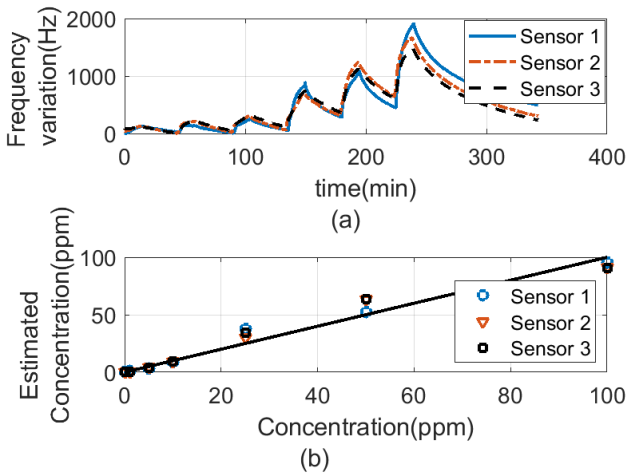

Fig. 23. Comparison of the response of the 3 sensors designed for the detection of high concentrations of up to 100 ppm NO_2. (a) Frequency variation as a function of time. (b) Estimated concentration for each sensor.

is a reduction of the tag's threshold power and consequently, of the reading range. The Voyantic Tagformance UHF RFID measurement system is used for measurements that study the variation of gain vs frequency, avoiding the use of commercial readers. Therefore, the practical application often requires the use of a reference tag without sensitive material to be detected using commercial readers. The measurement is also affected by multi-path interference. The gas concentration in the UHF sensors is relatively large to appreciate changes in the antenna response, therefore, these sensors can be mainly used to detect the presence or absence of the gas. The advantage is that the reading range reaches a few meters.

A similar approach based on tag detuning is presented in [63] at the 13.56 MHz band. In this case, the loop antenna is covered by a carbon polymer sensitive to NH_3 that changes the resonance frequency of the tag. Changes in resonance frequency are measured with a test coil antenna connected to a vector network analyzer (VNA). Therefore, these tags cannot be read with standard NFC readers. Another approach at 13.56 MHz is presented in [64], where a rectifier connected to the antenna coil tuned at 13.56 MHz is used to feed a ring oscillator, whose frequency is a function of the resistive gas sensor. The output of the oscillator modulates the antenna load. Therefore, the back-scattered signal has a sideband that depends on the gas concentration. This sensor requires a spectrum analyzer to measure the modulation frequency, and therefore it cannot be characterized by standard NFC readers unless modifications are made.

Another strategy consists in the use of the energy harvested from the incoming RF field to power the electronics necessary for sensing and use the RFID link to return the measured data. In [65], a batteryless RFID gas sensor based on a graphene gas sensor has been proposed. A UHF IC (ROCKY100 from FARSENS) with energy harvesting voltage output is used to supply a microcontroller whose ADCs read the output of a Wheatstone bridge. The readout data is saved in the EPC message and read with a standard UHF reader. However, a small range of concentrations can be detected using the proposed approach. In [66], an NFC IC is used for the communication, although a wireless power transfer link is additionally used to bias an Arduino microcontroller with the NFC shield. A battery-powered NFC sensor is presented in [67], where four commercial ULP metal oxide (MOX) sensors are connected with a switch to the signal conditioning potentiostat and transimpedance amplifier. The duty cycle is optimized to reduce power consumption and enlarge the battery lifetime.

A very different approach consists in chipless gas sensors such as those presented in [68]; here the sensitive material produces a shift in the resonance, which is measured with a vector network analyzer. In addition to the cost of using a VNA as a reader, the problem with chipless technology is that the electromagnetic response can be affected by surrounding objects and often a background subtraction calibration or special depolarizing tags are required to identify small variations.

Finally, in this work, a battery-less NFC sensor compatible with standard NFC readers, such as the ones present in smartphones (therefore, it does not require specialized readers such as expensive VNA or UHF RFID readers), has been developed to read resistive gas sensors based on the measurement of the frequency at the output of a variable oscillator that depends on the resistance of the sensor. This reading method allows a wide range of resistance variation to be measured compared to the Wheatstone bridge and no adjustments are necessary. The designed tag is a low-cost tag based on commercially-available off-the-shelf (COTS) components. Experimental results show that commercial smartphones are able to power up the tag without the need for other wireless power transfer systems such as in [66]. The readout method is not based on detuning the resonance frequency of the tag or the antenna, therefore it is not affected by the presence of multipath or metallic objects. A proof of concept that integrates NO_2 sensors is presented, capable of reading sub-ppm concentrations. Regarding response and recovery times, the sensors included in the table operate at room temperature, therefore the time response is slow compared to commercial sensors working at a high temperature, which need a heater that increases the current consumption and are therefore not suitable for battery-less applications. The tag can be employed with other chemiresistor sensors.

V. Conclusion and Future Work

In this work, it has been proposed to implement a low-cost LIG-based resistive gas sensor, which uses NFC technology for its wireless operation without the need for a battery. The tag is designed using commercially-available off-the-shelf (COTS) components and operates by harnessing energy of the NFC IC, which is obtained from the magnetic field generated by the reader. Since NFC readers are included in modern smartphones, no specific readers are needed, making this system accessible to the general population only by installing a specific mobile application (app). In the proof of concept, gas sensors to detect NO_2, based on laser-induced graphene have been employed. The sensors present good sensitivity at

TABLE II
COMPARISON TABLE OF RFID GAS SENSORS

Ref.	Battery-less	Communication Technology	Gas target	Range	Sensor Technology	Response time/recovery time
[58]	Yes	UHF RFID, tag detuning	NH_3	On/Off detection	SWCNT	15 nin/60 min
[59]	Yes	UHF RFID, tag detuning	NH_3	100 ppm	Ruthenium (Ru) doped zinc oxide nanostructure	6.5 s/15 s
[60]	Yes	UHF RFID, tag detuning	CO_2	On/OFF detection at 2600 ppm at 30 °C	CNT	200 s
[61]	Yes	UHF RFID, tag detuning	NO_2	0.2-100 ppm	carbon nanofiber (Fe2O3-MPCNF)	2 min
[62]	Yes	UHF RFID, tag detuning	H_2S	0.5-50 ppm	Fe2O3 hollow nanoparticles (M-FeHNPs) and PANI:PSS	2 min
[63]	Yes	resonance detuning at 13.56 MHz	NH_3	151 ppm	Carbon black/organic polymer	20 min
[64]	Yes	rectifier and FM modulation of 13.56 MHz carrier	NH_3	2-24 ppm	SWCNT	20 min
[65]	Yes	UHF RFID, microcontroler and Wheatstone bridge	NO_2	0.5-1 ppm	Graphene	15 min
[66]	Yes	NFC, wireless transfer power module	trimethylamine	1-10 ppm	WO_3/MXene	2 s/3 s
[67]	No	NFC	CO, NO_2, benzene, acetaldehyde	2-50 ppm	ULP Metal Oxide (MOX) SNO_2	2 s/12 min
[68]	Yes	chipless, 1780 MHz, resonator detuning	NO_2	0.5-5 ppm	SnO_2 nanoparticles	28 min/1000 min
This work	Yes	NFC with energy harvesting	NO_2	50 ppb-1 ppm and 0.5-100 ppm	LIG	6.8-8 min/44 min

room temperature and operate without bias, they also show strong selectivity to NO_2 compared to other gases such as CO, NH_3, H_2, and H_2S. The sensor's reading mechanism relies on measuring the oscillation frequency of a low-power timer oscillator. This method eliminates the need to adjust the gain and allows sensors with different resistance ranges to be used. The baseline and gain sensitivity are stored in the internal memory of the tag, facilitating a quick sensor installation and calibration. The collected data can be uploaded to various databases based on the application requirement, enabling valuable data analysis. This feature opens the door to a wide range of distributed applications in environmental control, personal safety, or logistics using the collaboration of the users and public wireless networks to collect and utilize the data. Looking to the future, there is potential to make further advances in battery-free LIG-based sensors by investigating the methods to control the selectivity and enhance the sensitivity to various gases. This is especially promising considering the numerous reports on different applications of graphene in gas sensing. Such developments may lead to even more versatile and cost-effective gas-sensing solutions with a wider range of applications.

REFERENCES

[1] J. A. Paradiso and T. Starner, "Energy scavenging for mobile and wireless electronics," *IEEE Pervasive computing*, vol. 4, no. 1, pp. 18–27, 2005.

[2] E. M. Melchor-Martínez, R. Macias-Garbett, A. Malacara-Becerra, H. M. Iqbal, J. E. Sosa-Hernández, and R. Parra-Saldívar, "Environmental impact of emerging contaminants from battery waste: A mini review," *Case Studies in Chemical and Environmental Engineering*, vol. 3, p. 100104, 2021.

[3] W. Mrozik, M. A. Rajaeifar, O. Heidrich, and P. Christensen, "Environmental impacts, pollution sources and pathways of spent lithium-ion batteries," *Energy & Environmental Science*, vol. 14, no. 12, pp. 6099–6121, 2021.

[4] G. U. Adie and O. Osibanjo, "Assessment of soil-pollution by slag from an automobile battery manufacturing plant in Nigeria," *African Journal of Environmental Science and Technology*, vol. 3, no. 9, 2009.

[5] W. Li, Q. Liu, Y. Zhang, C. Li, Z. He, W. C. Choy, P. J. Low, P. Sonar, and A. K. K. Kyaw, "Biodegradable materials and green processing for green electronics," *Advanced materials*, vol. 32, no. 33, p. 2001591, 2020.

[6] N. R. Misra, S. Kumar, and A. Jain, "A review on E-waste: Fostering the need for green electronics," in *2021 International Conference on Computing, Communication, and Intelligent Systems (ICCCIS)*. IEEE, 2021, pp. 1032–1036.

[7] H. Duan, Q. Huang, Q. Wang, B. Zhou, and J. Li, "Hazardous waste generation and management in China: A review," *Journal of hazardous materials*, vol. 158, no. 2-3, pp. 221–227, 2008.

[8] P. Moravek, D. Komosny, M. Simek, D. Girbau, and A. Lazaro, "Energy Analysis of Received Signal Strength Localization in Wireless Sensor Networks," *Radioengineering*, vol. 20, no. 4, 2011.

[9] T. A. Alghamdi, "Energy efficient protocol in wireless sensor network: optimized cluster head selection model," *Telecommunication Systems*, vol. 74, pp. 331–345, 2020.

[10] J. Amutha, S. Sharma, and S. K. Sharma, "Strategies based on various aspects of clustering in wireless sensor networks using classical, optimization and machine learning techniques: Review, taxonomy, research findings, challenges and future directions," *Computer Science Review*, vol. 40, p. 100376, 2021.

[11] M. Bal, "Industrial applications of collaborative wireless sensor networks: A survey," in *2014 IEEE 23rd international symposium on industrial electronics (ISIE)*. IEEE, 2014, pp. 1463–1468.

[12] J. Wu, S. Yuan, S. Ji, G. Zhou, Y. Wang, and Z. Wang, "Multi-agent system design and evaluation for collaborative wireless sensor network in large structure health monitoring," *Expert Systems with Applications*, vol. 37, no. 3, pp. 2028–2036, 2010.

[13] A. Amin, X.-H. Liu, M. A. Saleem, S. Henna, T.-u. Islam, I. Khan, P. Uthansakul, M. Z. Qurashi, S. S. Mirjavadi, and M. Forsat, "Collaborative wireless power transfer in wireless rechargeable sensor networks," *Wireless Communications and Mobile Computing*, vol. 2020, 2020.

[14] V. Gupta and S. De, "Collaborative multi-sensing in energy harvesting

wireless sensor networks," *IEEE Transactions on Signal and Information Processing over Networks*, vol. 6, pp. 426–441, 2020.

[15] A. Lazaro, R. Villarino, and D. Girbau, "A survey of NFC sensors based on energy harvesting for IoT applications," *Sensors*, vol. 18, no. 11, p. 3746, 2018.

[16] M. Boada, A. Lazaro, R. Villarino, and D. Girbau, "Battery-less soil moisture measurement system based on a nfc device with energy harvesting capability," *IEEE Sensors Journal*, vol. 18, no. 13, pp. 5541–5549, 2018.

[17] A. Lazaro, M. Boada, R. Villarino, and D. Girbau, "Color measurement and analysis of fruit with a battery-less NFC sensor," *Sensors*, vol. 19, no. 7, p. 1741, 2019.

[18] A. Lazaro, M. Boada, and R. Villarino, "Battery–Less Smart Diaper Based on NFC Technology," *IEEE Sensors Journal*, vol. 19, no. 22, pp. 10 848–10 858, 2019.

[19] M. Boada, A. Lazaro, R. Villarino, E. Gil-Dolcet, and D. Girbau, "Battery-less NFC bicycle tire pressure sensor based on a force-sensing resistor," *IEEE Access*, vol. 9, pp. 103 975–103 987, 2021.

[20] P. Escobedo, M. M. Erenas, A. Martinez-Olmos, M. A. Carvajal, S. Gonzalez-Chocano, L. F. Capitán-Vallvey, and A. J. Palma, "General-purpose passive wireless point–of–care platform based on smartphone," *Biosensors and Bioelectronics*, vol. 141, p. 111360, 2019.

[21] A. Lazaro, R. Villarino, M. Lazaro, N. Canellas, B. Prieto-Simon, and D. Girbau, "Battery-Less NFC Potentiostat for Electrochemical Point-of-Care Sensors Based on COTS Components," *Sensors*, vol. 22, no. 19, p. 7213, 2022.

[22] K. Promsuwan, A. Soleh, K. Samoson, K. Saisahas, S. Wangchuk, J. Saichanapan, P. Kanatharana, P. Thavarungkul, and W. Limbut, "Novel biosensor platform for glucose monitoring via smartphone based on battery-less NFC potentiostat," *Talanta*, p. 124266, 2023.

[23] A. Lazaro, R. Villarino, M. Lazaro, N. Canellas, B. Prieto-Simon, and D. Girbau, "Recent Advances in Batteryless NFC Sensors for Chemical Sensing and Biosensing," *Biosensors*, vol. 13, no. 8, 2023. [Online]. Available: https://www.mdpi.com/2079-6374/13/8/775

[24] S. Zhang, M. A. Zahed, M. Sharifuzzaman, S. Yoon, X. Hui, S. C. Barman, S. Sharma, H. S. Yoon, C. Park, and J. Y. Park, "A wearable battery-free wireless and skin-interfaced microfluidics integrated electrochemical sensing patch for on-site biomarkers monitoring in human perspiration," *Biosensors and Bioelectronics*, vol. 175, p. 112844, 2021.

[25] R. Rahimi, U. Brener, M. Ochoa, and B. Ziaie, "Flexible and transparent pH monitoring system with NFC communication for wound monitoring applications," in *2017 IEEE 30th international conference on micro electro mechanical systems (MEMS)*. IEEE, 2017, pp. 125–128.

[26] H. M. Jarvis DJ, Adamkiewicz G. (2010) Nitrogen dioxide. [Online]. Available: https://www.ncbi.nlm.nih.gov/books/NBK138707/

[27] W. Tsujita, A. Yoshino, H. Ishida, and T. Moriizumi, "Gas sensor network for air-pollution monitoring," *Sensors and Actuators B: Chemical*, vol. 110, no. 2, pp. 304–311, 2005.

[28] D. Sun, Y. Luo, M. Debliquy, and C. Zhang, "Graphene-enhanced metal oxide gas sensors at room temperature: A review," *Beilstein journal of nanotechnology*, vol. 9, no. 1, pp. 2832–2844, 2018.

[29] E. Singh, M. Meyyappan, and H. S. Nalwa, "Flexible graphene-based wearable gas and chemical sensors," *ACS applied materials & interfaces*, vol. 9, no. 40, pp. 34 544–34 586, 2017.

[30] K. E. Whitener Jr and P. E. Sheehan, "Graphene synthesis," *Diamond and related materials*, vol. 46, pp. 25–34, 2014.

[31] J. Lin, Z. Peng, Y. Liu, F. Ruiz-Zepeda, R. Ye, E. L. Samuel, M. J. Yacaman, B. I. Yakobson, and J. M. Tour, "Laser-induced porous graphene films from commercial polymers," *Nature communications*, vol. 5, no. 1, p. 5714, 2014.

[32] R. Ye, D. K. James, and J. M. Tour, "Laser-induced graphene," *Accounts of chemical research*, vol. 51, no. 7, pp. 1609–1620, 2018.

[33] L. X. Duy, Z. Peng, Y. Li, J. Zhang, Y. Ji, and J. M. Tour, "Laser-induced graphene fibers," *Carbon*, vol. 126, pp. 472–479, 2018.

[34] F. M. Vivaldi, A. Dallinger, A. Bonini, N. Poma, L. Sembranti, D. Biagini, P. Salvo, F. Greco, and F. Di Francesco, "Three-dimensional (3D) laser-induced graphene: structure, properties, and application to chemical sensing," *ACS Applied Materials & Interfaces*, vol. 13, no. 26, pp. 30 245–30 260, 2021.

[35] L. Cheng, W. Guo, X. Cao, Y. Dou, L. Huang, Y. Song, J. Su, Z. Zeng, and R. Ye, "Laser-induced graphene for environmental applications: progress and opportunities," *Materials Chemistry Frontiers*, vol. 5, no. 13, pp. 4874–4891, 2021.

[36] J. Zhao, N. Yi, X. Ding, S. Liu, J. Zhu, A. C. Castonguay, Y. Gao, L. D. Zarzar, and H. Cheng, "In situ laser-assisted synthesis and patterning of graphene foam composites as a flexible gas sensing platform," *Chemical Engineering Journal*, vol. 456, p. 140956, 2023.

[37] S.-F. Tseng, P.-S. Chen, S.-H. Hsu, W.-T. Hsiao, and W.-J. Peng, "Investigation of fiber laser-induced porous graphene electrodes in controlled atmospheres for ZnO nanorod-based NO2 gas sensors," *Applied Surface Science*, vol. 620, p. 156847, 2023.

[38] L. Yang, G. Zheng, Y. Cao, C. Meng, Y. Li, H. Ji, X. Chen, G. Niu, J. Yan, Y. Xue *et al.*, "Moisture-resistant, stretchable NOx gas sensors based on laser-induced graphene for environmental monitoring and breath analysis," *Microsystems & nanoengineering*, vol. 8, no. 1, p. 78, 2022.

[39] L. Yang, N. Yi, J. Zhu, Z. Cheng, X. Yin, X. Zhang, H. Zhu, and H. Cheng, "Novel gas sensing platform based on a stretchable laser-induced graphene pattern with self-heating capabilities," *Journal of materials chemistry A*, vol. 8, no. 14, pp. 6487–6500, 2020.

[40] A. De Marcellis, G. Ferri, and P. Mantenuto, "Analog Wheatstone bridge-based automatic interface for grounded and floating wide-range resistive sensors," *Sensors and Actuators B: Chemical*, vol. 187, pp. 371–378, 2013.

[41] NFC Forum, "NFC Data Exchange Format (NDEF)," 2006.

[42] T. Igoe, D. Coleman, and B. Jepson, *Beginning NFC: near field communication with Arduino, Android, and Phonegap*. " O'Reilly Media, Inc.", 2014.

[43] J. Santos, "LaserSimulationLIG," https://https://github.com/jcsantosc/laserSimulationLIG, 2023.

[44] A. Mostaccio, G. Antonelli, M. Bragaglia, E. Martinelli, and G. Marrocco, "Comparative Evaluation of Laser Induced Graphene (LIG) Traces on Polyimide under Soft and Hard Stress for IoT Applications," *IEEE Journal on Flexible Electronics*, 2023.

[45] B. D. Abera, I. Ortiz-Gómez, B. Shkodra, F. J. Romero, G. Cantarella, L. Petti, A. Salinas-Castillo, P. Lugli, and A. Rivadeneyra, "Laser-induced graphene electrodes modified with a molecularly imprinted polymer for detection of tetracycline in milk and meat," *Sensors*, vol. 22, no. 1, p. 269, 2021.

[46] N. Chatterjee, B. Bhattacharyya, D. Dey, and S. Munshi, "A combination of astable multivibrator and microcontroller for thermistor-based temperature measurement over internet," *IEEE Sensors Journal*, vol. 19, no. 9, pp. 3252–3259, 2019.

[47] R. Anandanatarajan, U. Mangalanathan, and U. Gandhi, "Enhanced Microcontroller Interface of Resistive Sensors Through Resistance-to-Time Converter," *IEEE Transactions on Instrumentation and Measurement*, vol. 69, no. 6, pp. 2698–2706, 2020.

[48] P. Klomklao, S. Kuntinugunetanon, and W. Wongkokua, "Moisture content measurement in paddy," in *Journal of Physics: Conference Series*, vol. 901, no. 1. IOP Publishing, 2017, p. 012068.

[49] A. Arshad, R. Tasnim, A. Z. Alam, and S. Khan, "Capacitance-to-voltage converter design to measure small change in capacitance produced by human body movement," in *2015 IEEE International WIE Conference on Electrical and Computer Engineering (WIECON-ECE)*. IEEE, 2015, pp. 114–117.

[50] S. Milici, J. Lorenzo, A. Lazaro, R. Villarino, and D. Girbau, "Wireless breathing sensor based on wearable modulated frequency selective surface," *IEEE Sensors Journal*, vol. 17, no. 5, pp. 1285–1292, 2016.

[51] H. M. Bertin and C. Gould, "The 555 Timer: Applications Sourcebook With Experiments," 1977.

[52] S. Barrett and D. Pack, "Atmel avr microcontroller primer: Programming and interfacing," *Synthesis Lectures on Digital Circuits and Systems*, vol. 7, no. 2, pp. 1–244, 2012.

[53] M. Gebhart, "Analytical considerations for an ISO/IEC14443 compliant SmartCard transponder," in *Proceedings of the 11th International Conference on Telecommunications*, 2011, pp. 9–16.

[54] A. Lazaro, M. Boada, R. Villarino, and D. Girbau, "Study on the reading of energy-harvested implanted NFC tags using mobile phones," *IEEE Access*, vol. 8, pp. 2200–2221, 2019.

[55] H. A. Wheeler, "Simple inductance formulas for radio coils," *Proceedings of the institute of Radio Engineers*, vol. 16, no. 10, pp. 1398–1400, 1928.

[56] A. Lazaro, R. Villarino, M. Lazaro, N. Canellas, B. Prieto-Simon, and D. Girbau, "Battery-Less NFC Potentiostat for Electrochemical Point-of-Care Sensors Based on COTS Components," *Sensors*, vol. 22, no. 19, p. 7213, 2022.

[57] T. Pham, G. Li, E. Bekyarova, M. E. Itkis, and A. Mulchandani, "MoS2-based optoelectronic gas sensor with sub-parts-per-billion limit of NO2 gas detection," *ACS nano*, vol. 13, no. 3, pp. 3196–3205, 2019.

[58] C. Occhiuzzi, A. Rida, G. Marrocco, and M. Tentzeris, "RFID Passive Gas Sensor Integrating Carbon Nanotubes," *IEEE Transactions on Microwave Theory and Techniques*, vol. 59, no. 10, pp. 2674–2684, 2011.

[59] I. Ali, A. E.-H. B. Kashyout, M. Tayel, H. S. Hassan, and M. Rizk, "Ruthenium (Ru) doped zinc oxide nanostructure-based radio frequency identification (RFID) gas sensors for NH3 detection," *Journal of Materials Research and Technology*, vol. 9, no. 6, pp. 15 693–15 704, 2020.
[60] A. A. Kutty, T. Björninen, L. Sydänheimo, and L. Ukkonen, "A novel carbon nanotube loaded passive UHF RFID sensor tag with built-in reference for wireless gas sensing," in *2016 IEEE MTT-S International Microwave Symposium (IMS)*, 2016, pp. 1–4.
[61] S. G. Kim, J. Jun, J. S. Lee, and J. Jang, "A highly sensitive wireless nitrogen dioxide gas sensor based on an organic conductive nanocomposite paste," *Journal of materials chemistry A*, vol. 7, no. 14, pp. 8451–8459, 2019.
[62] S. G. Kim, T. V. Tran, and J. S. Lee, "Iron oxide-immobilized porous carbon nanofiber-based radio frequency identification (RFID) tag sensor for detecting hydrogen sulfide," *Journal of Industrial and Engineering Chemistry*, vol. 112, pp. 423–429, 2022.
[63] L. K. Fiddes and N. Yan, "Rfid tags for wireless electrochemical detection of volatile chemicals," *Sensors and Actuators B: Chemical*, vol. 186, pp. 817–823, 2013.
[64] Y. Ling, H. Zhang, G. Gu, X. Lu, V. Kayastha, C. S. Jones, W.-S. Shih, and D. C. Janzen, "A Printable CNT-Based FM Passive Wireless Sensor Tag on a Flexible Substrate With Enhanced Sensitivity," *IEEE Sensors Journal*, vol. 14, no. 4, pp. 1193–1197, 2014.
[65] A. Estevez, N. Perez, J. Casanova-Chafer, E. Llobet, and A. Beriain, "RFID Gas Sensor for In-field Detection of Chemical Threats: Evaluation of batteryless discontinuous operation," in *2022 IEEE Sensors*. IEEE, 2022, pp. 1–4.
[66] Z. Li, D. Zhang, X. Wang, X. Liu, Y. Yang, C. Du, J. Guo, and Y. Zhang, "Passive and Wireless NFC Tag-Type Trimethylamine Gas Detection Based on WO3/MXene Composite Sensors," *Journal of Alloys and Compounds*, p. 168730, 2023.
[67] F. Palacio, J. Fonollosa, J. Burgués, J. M. Gomez, and S. Marco, "Pulsed-temperature metal oxide gas sensors for microwatt power consumption," *IEEE access*, vol. 8, pp. 70 938–70 946, 2020.
[68] V. Mulloni, A. Gaiardo, G. Marchi, M. Valt, L. Vanzetti, M. Donelli, and L. Lorenzelli, "Sub-ppm NO2 Detection through Chipless RFID Sensor Functionalized with Reduced SnO2," *Chemosensors*, vol. 11, no. 7, p. 408, 2023.

Foad Salehnia was born in Sanandaj, Iran. He completed his Ph.D. in Nanochemistry at the University of Tehran in 2019. He subsequently pursued two postdoctoral positions at the same university. He is a Maria Zambrano research fellow at the MINOS research group at the University of Rovira i virgili Tarragona, Spain. His research interests focus on synthesizing novel carbon-based nanomaterials and investigating their applications in sensing areas and energy conversion systems.

Antonio Lazaro (M'07–SM'16) was born in Lleida, Spain, in 1971. He received the M.S. and Ph.D. degrees in telecommunication engineering from the Universitat Politècnica de Catalunya (UPC), Barcelona, Spain, in 1994 and 1998, respectively. He then joined the faculty of UPC, where he currently teaches a course on microwave circuits and antennas. Since July 2004, he is a Full-Time Professor at the Department of Electronic Engineering, Universitat Rovira i Virgili (URV), Tarragona, Spain. His research interests are microwave device modeling, on-wafer noise measurements, monolithic microwave integrated circuits (MMICs), low phase noise oscillators, MEMS, RFID, UWB and microwave systems.

Marc Lazaro was born in Tarragona, Spain, in 1995. He received the BS in Industrial Electronics and Automation Engineering and the MS in Electronic Systems Engineering and Technology (METSE) from Rovira i Virgili University, Tarragona, Spain, in 2017 and 2018, respectively. Up until now, he has accumulated professional experience as a data acquisition engineer and as embedded systems developer. Since 2019 he has been working toward the Ph.D. degree in the Department of Electronics at the Rovira i Virgili University. His research activities are focused on semipassive RFID technologies based on backscattering communication and novel applications based on Millimeter wave identification (MMID).

Ramon Villarino was awarded a degree in Telecommunications Technical Engineering by Ramon Llull University (URL) in Barcelona, Spain, in 1994, a degree in Senior Telecommunications Engineering by the Universitat Politècnica de Catalunya (UPC) in Barcelona, Spain, in 2000 and a doctorate by the UPC in 2004. In 2005-2006, he was a Research Associate at the Technological Telecommunications Center of Catalonia (CTTC) in Barcelona, Spain. He worked as a Researcher and Assistant Professor at the Universitat Autònoma de Barcelona (UAB) from 2006 to 2008. Since January 2009 he has been a full-time professor at Universitat Rovira i Virgili (URV) in Tarragona, Spain. His research activities focus on radiometry, microwave devices, and systems based on UWB, RFIDs, and frequency selective structures using MetaMaterials (MM).

Nicolas Canyellas obtained his PhD from the Rovira i Virgili University in Tarragoan, Spain, 2006, where he currenty holds a position as an associate professor. He started working on hardware / software co-design for biometric pattern recognition issues. In 2006 he joined MINOS/SIPOMICS research group and his research interests moved to the metabolomics field, where he is currently working in the development of advanced tools for 1H-NMR data analysis and signal processing and data analysis methods to facilitate the discovery of biomarkers by metabolic techniques.

Xavier Vilanova received the Ph.D. from the Universitat Politecnica de Catalunya(UPC-Barcelona, Spain) in 1998. Since 2010, he is a Full Professor of Electronics Technology with the Universitat Rovira i Virgili, Tarragona, Spain. His research interests comprise gaining insight in the information extracted from gas sensors transients when exposed to pulsed light excitation. He is also working in developing scalable and low cost processes to obtain flexible gas sensors.

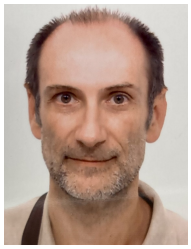

Eduard Llobet (Senior Member, IEEE) received the Ph.D. degree from UPC (Bercelona) in 1997. He completed a one-year postdoc with the University of Warwick, U.K. He is a Full Professor of Electronics with the Universitat Rovira i Virgili, Tarragona, Spain. His research interests comprise gaining insight in the surface chemistry, nature of defects and the specific mechanisms of the interaction of metal oxides, transition metal dichacogenides and carbon nanomaterials with target gases, unveiling gas-sensing mechanisms and structure-performance relationships. He is also working towards the realization of nanomaterial-based flexible gas sensors and sensor systems with a performance that matches the one of conventional rigid devices.

David Girbau (M'04–SM'13) was awarded a BSc in Telecommunication Engineering, a Master's in Electronics Engineering, and a doctorate in Telecommunication by Universitat Politècnica de Catalunya (UPC) in Barcelona, Spain, in 1998, 2002 and 2006, respectively. From February 2001 to September 2007 he was a Research Assistant at UPC. From September 2005 to September 2007 he was a part-time Assistant Professor at Universitat Autònoma de Barcelona (UAB). Since October 2007 he has been a full-time professor at Universitat Rovira i Virgili (URV) in Tarragona, Spain. His research interests include microwave devices and systems, with an emphasis on UWB, RFIDs, RF-MEMS and wireless sensors.